

UC Davis
IDAV Publications

Title

Generalizing lifted Tensor-Product Wavelets to Irregular Polygonal Domains

Permalink

<https://escholarship.org/uc/item/6h87q67b>

Authors

Bertram, Martin
Duchaineau, Mark A.
Hamann, Bernd
[et al.](#)

Publication Date

2003

Peer reviewed

GENERALIZING LIFTED TENSOR-PRODUCT WAVELETS TO IRREGULAR POLYGONAL DOMAINS

Martin Bertram

University of Kaiserslautern

bertram@informatik.uni-kl.de

Mark A. Duchaineau

Lawrence Livermore National Laboratory

duchaine@llnl.gov

Bernd Hamann

University of California at Davis and Lawrence Berkeley National Laboratory

hamann@cs.ucdavis.edu

Kenneth I. Joy

University of California at Davis

joy@cs.ucdavis.edu

Keywords: Approximation, B-Splines, Geometry Compression, Lifting, Subdivision Surfaces, Tessellations, Wavelets

Abstract We present a new construction approach for symmetric lifted B-spline wavelets on irregular polygonal control meshes defining two-manifold topologies. Polygonal control meshes are recursively refined by stationary subdivision rules and converge to piecewise polynomial limit surfaces. At every subdivision level, our wavelet transforms provide an efficient way to add geometric details that are expanded from wavelet coefficients. Both wavelet decomposition and reconstruction operations are based on local lifting steps and have linear-time complexity.

1. INTRODUCTION

Biorthogonal wavelet transforms, see Stollnitz *et al.* (1996), are used for compression of scientific data, progressive transmission, hierarchical modeling, and solving diverse numerical problems. Wavelets are useful in computer-aided geometric design (CAGD) to represent surfaces at different levels of resolution for visualization and design purposes. Highly complex functions, like flow fields or terrain models, are transformed into a sparse wavelet basis within linear computation time. Quantization and arithmetic coding of wavelet coefficients leads to high compression rates at the expense of relatively small reconstruction errors. Lossless compression is possible for data represented in form of integer or finite-precision samples.

A challenge of recent interest is the construction of wavelets on non-planar, two-manifold domain topologies, like spherical domains, see Schröder/Sweldens (1995), or general two-manifolds of arbitrary genus, see Lounsbery *et al.* (1997) and Stollnitz *et al.* (1996). We present a new construction approach generalizing biorthogonal tensor-product wavelets defined on planar domains to *subdivision surfaces* of arbitrary topology. The novelty of our wavelet approach is that both, the transform and its inverse are computed by local operations. Previous wavelet constructions for smooth, non-interpolating subdivision surfaces require the solution of a sparse linear system for computing the wavelet transform, see Stollnitz *et al.* (1996), whereas the inverse transform is computed locally.

Subdivision surfaces are defined by polygonal base meshes that are recursively subdivided according to regular refinement rules converging to continuous limit surfaces. The first subdivision surfaces reproducing piecewise polynomials were described by Catmull/Clark (1978) and Doo/Sabin (1978). Surface boundaries and sharp features can be represented by modified subdivision and fitting rules, see Biermann *et al.* (2000). Our approach is based on *wavelet lifting*, introduced by Sweldens (1996), which simplifies the construction of basis functions, accelerates the computation of the wavelet transform, and is suitable for the use of integer arithmetic to obtain lossless compression, see Bertram (2000).

2. WAVELET CONSTRUCTION

Wavelets have their roots in signal processing. A function is transformed by recursively separating *details*, corresponding to the highest frequency band, from the remaining lower frequencies. In geometric modeling applications, this filtering corresponds to a fitting operation \mathbf{F} projecting a function onto a smaller space spanned by coarser (lower-

frequency) basis functions. The removed details, *i.e.*, the differences between the fit and the original function, are transformed into wavelet coefficients by a compaction-of-difference operator \mathbf{C} . This process is recursively applied, resulting in multiple levels of resolution, see Figure 1.

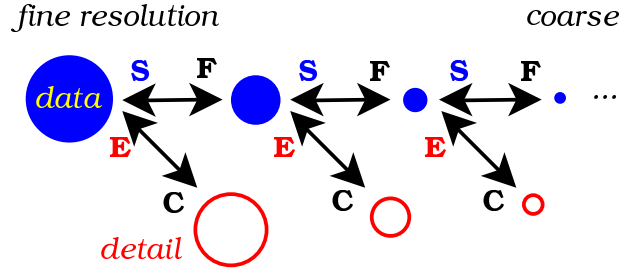


Figure 1 Multiresolution modeling paradigm of a wavelet transform. The fitting operator \mathbf{F} provides a coarser approximation of the data and the operator \mathbf{C} compactly stores the geometric details removed by \mathbf{F} .

The operators \mathbf{F} and \mathbf{C} are both linear transforms reducing the number of coefficients. Neither \mathbf{F} , nor \mathbf{C} have an inverse, when computed separately. The combination of \mathbf{F} and \mathbf{C} , however, is inverted by a subdivision operator \mathbf{S} and an expansion-of-difference operator \mathbf{E} . In particular, \mathbf{F} is the inverse of \mathbf{S} and \mathbf{C} is the inverse of \mathbf{E} .

We start with constructing wavelets in one dimension by defining the operators \mathbf{S} and \mathbf{E} . These operators already determine the shape of the basis functions (wavelets representing details and *scaling functions* representing the individual levels of resolution). The construction is done in a way such that the filtering operations for \mathbf{S} and \mathbf{E} are factorized into smallest possible lifting operations that are symmetric and involve only three coefficients at a time, see Figure 2. There can be an arbitrary number of these lifting steps. Examples for linear and cubic B-spline wavelet constructions are provided in the Appendix.

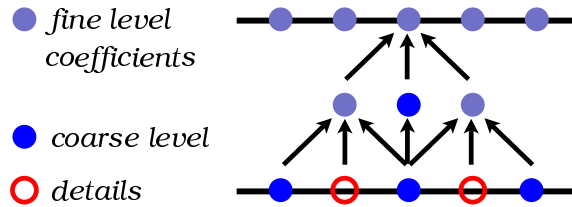


Figure 2 Factoring the computation of \mathbf{S} and \mathbf{E} into small lifting steps. Circles represent individual coefficients at certain stages of the transform, whereas arrows denote the dependencies.

On surfaces defined by regular, rectilinear control meshes, our lifted one-dimensional wavelet transform is applied independently to the rows and columns of the meshes, resulting in tensor-product basis functions. The number of control points is quadrupled in every subdivision step. This subdivision process is generalized to irregular base meshes by a subdivision hierarchy like Catmull-Clark surfaces, illustrated in Figure 3.

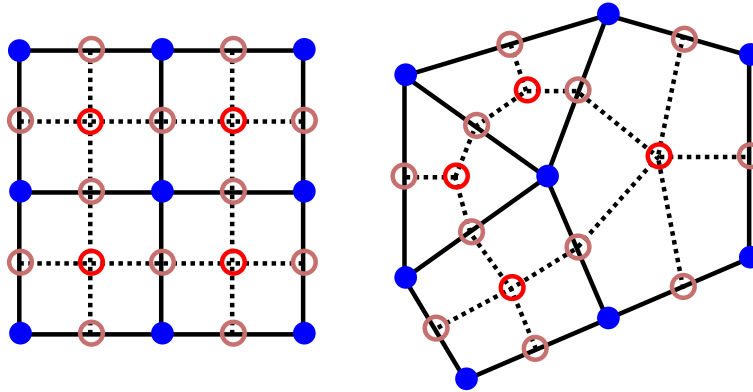


Figure 3 Regular subdivision of a rectilinear and an irregular mesh by inserting new vertices for every edge and for every polygon.

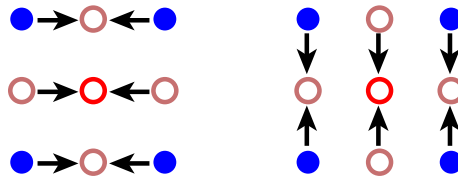


Figure 4 Tensor-product approach for one lifting operation. The coefficients in every second row/column are modified using values from the neighboring rows/columns.

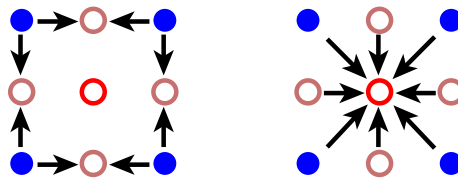


Figure 5 Same lifting operation as in Figure 4, but computed in different order. The coefficient located in the middle (corresponding to one out of four coefficients in a regular mesh) is updated only once by adding a linear combination of its eight neighbors.

On a regular rectilinear grid, the transform is independent of the order in which the operations are applied with respect to the canonical directions. Thus, we can compute every individual lifting operation for both directions subsequently, which is shown in Figure 4. Instead of updating the middle control point twice (for every canonical direction), we can change the order of computation such that every control point is updated only once, see Figure 5. The modified computation can be generalized to irregular base meshes. If the middle control point is extraordinary, *i.e.*, it has $n \neq 4$ incident edges, then we multiply the weights for its update by $\frac{4}{n}$ such that the total weight of points added remains independent of the valence n . The entire wavelet transform is computed by generalizing every individual lifting operation in this way.

The two-dimensional scaling functions can be obtained by setting the ordinate of only one control point to one and by applying the subdivision operator \mathbf{S} *ad infinitum*. The wavelets corresponding to control points located on edges or polygons of a certain-resolution mesh are defined by applying operator \mathbf{E} one time at this level and then operator \mathbf{S} *ad infinitum*. Boundary curves and sharp feature lines are treated differently by applying the lifting operations of the one-dimensional case along the corresponding edges in the mesh for all vertices located on these edges. Examples for recursively generated basis functions are illustrated in Figure 6.

We note that our mesh subdivision strategy generates only quadrilaterals and the number of extraordinary vertices remains constant after the first subdivision on an irregular mesh. Thus, most of the basis functions are located in rectilinear mesh regions and are tensor products. In the case of subdivision rules generating piecewise polynomials by dyadic refinement, see Duchaineau (1996), the generated basis functions are composed of polynomial patches that can be evaluated at arbitrary parameter values, even in the neighborhood of extraordinary points where the patches become smaller and smaller, see Stam (1998). The degree of continuity of subdivision surfaces at extraordinary points depends on the *eigenstructure* of local subdivision matrices. The limit surfaces of our bicubic subdivision scheme are C^1 -continuous at these points, see Peters/Reif (1998). We have constructed wavelets based on linear, cubic, and quintic B-spline subdivision, see Bertram (2000). A variety of different symmetric wavelets can be constructed and generalized to irregular meshes using this approach.

So far, we have only defined the inverse wavelet transform. The operators \mathbf{F} and \mathbf{C} for the wavelet transform are obtained by applying the inverse of every individual lifting step in reverse order. The input of the wavelet transform is a base mesh with subdivision hierarchy and valid

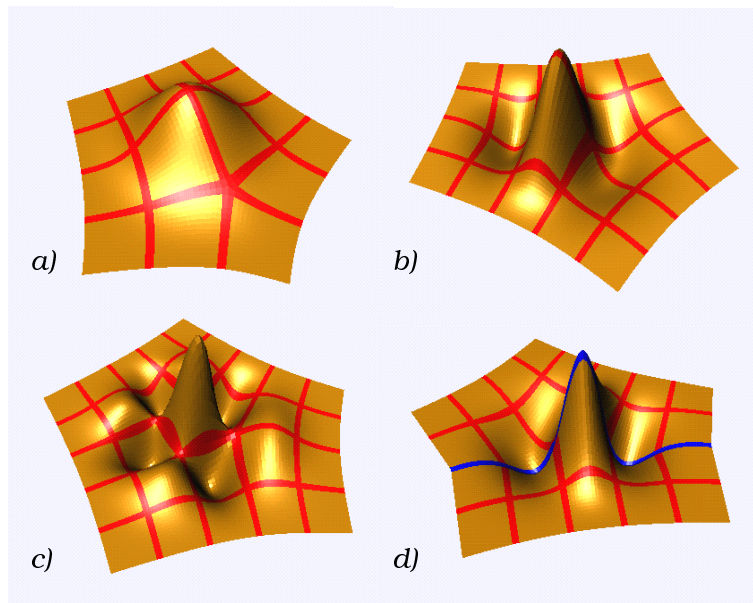


Figure 6 Generalized tensor-product basis functions resulting from generalized bicubic B-spline subdivision. a) scaling function; b) wavelet located on edge; c) wavelet located on polygon; d) wavelet with a sharp feature.

control points on a certain (finest) level of subdivision. The transform recursively computes a set of coarser approximation levels representing the differences between consecutive levels in form of sets of sparse wavelet coefficients. The coarsest level is defined by the control points of the irregular base mesh.

3. EXAMPLES

Our wavelet constructions for surfaces defined by irregular base meshes are applicable to a variety of problems. Some of the most significant applications for our technique are:

- Compression and progressive transmission of complex geometries, like isosurfaces extracted from computational fluid dynamics (CFD) simulations.
- View-dependent visualization of surfaces and of functions defined on surfaces, like texture maps, bump maps, and opacity. Geometric detail can be added locally to a surface, providing highest resolutions in visible areas close to the view point. An adaptive

mesh structure supporting this kind of local refinement was presented by Duchaineau *et al.* (1997).

- Sparse representation of functions defined on tessellated domains for scattered data approximation or radiosity solutions.

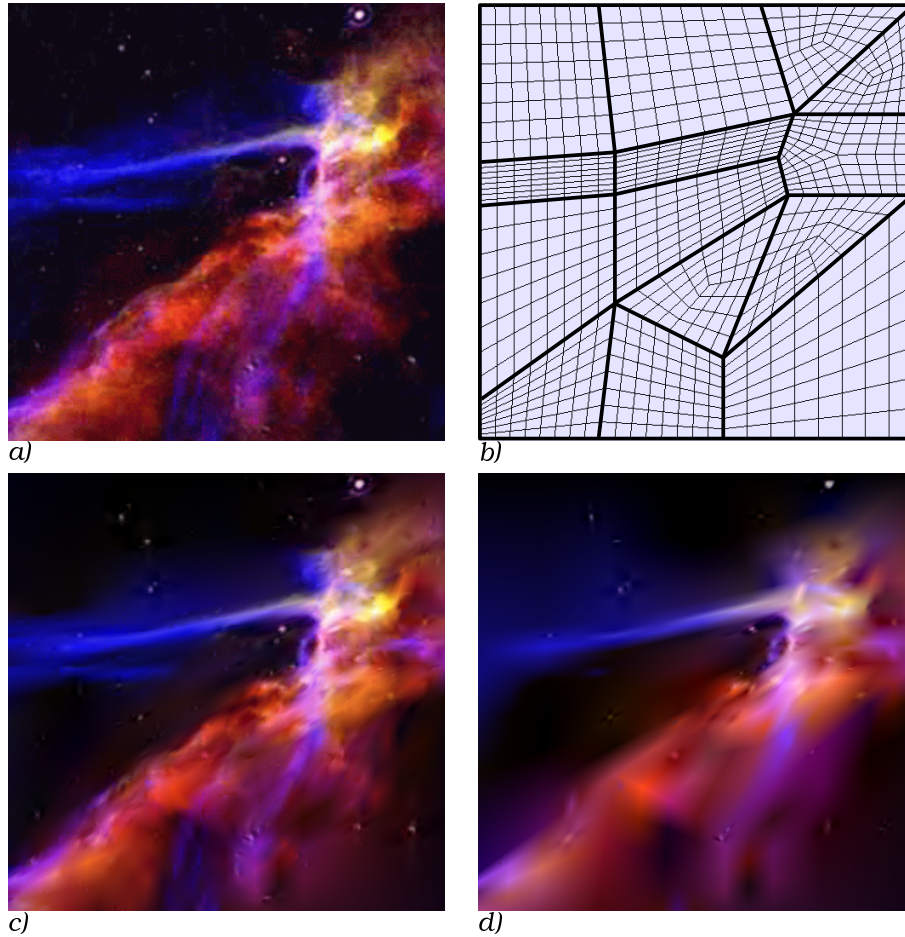


Figure 7 Generalized bilinear B-spline wavelet transform for a tessellated image. a) image resampled on subdivided tessellation (217921 samples); b) initial tessellation of image region; c) reconstruction from 1 percent of wavelet coefficients; d) reconstruction from 0.1 percent (218 coefficients).

An example for generalized bilinear B-spline wavelets defined on a tessellation is shown in Figure 7. Starting with a coarse tessellation of the “Cygnus Loop” Hubble image, courtesy of NASA, we have recur-

sively subdivided this tessellation seven times and re-sampled the image on the resulting mesh (217921 samples). Figure 7 shows reconstructions obtained by considering wavelet coefficients whose magnitudes are greater than a certain threshold. For more details about wavelets defined on tessellations we refer to Bertram *et al.* (2000a).

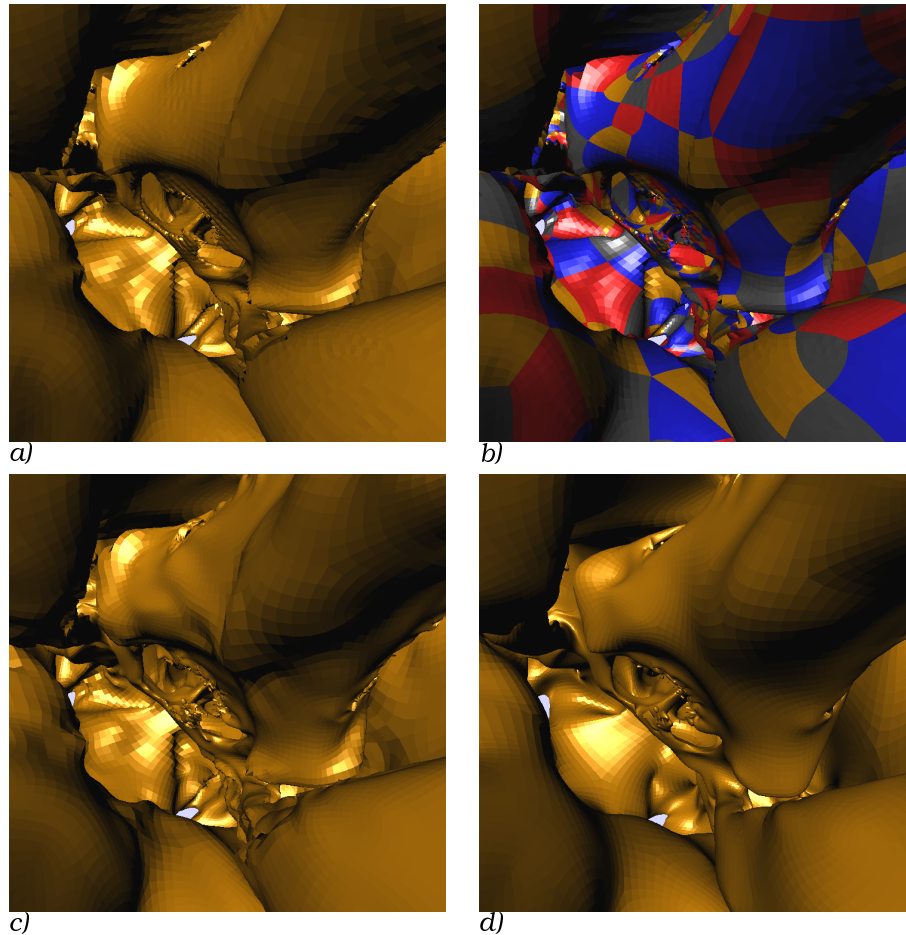


Figure 8 Generalized bicubic B-spline wavelets representing an isosurface. a) Local view of the isosurface resampled on a subdivided base mesh (1187277 control points); b) patches corresponding to base-mesh polygons shown in four different colors; c) reconstruction from 5 percent of wavelet coefficients; d) reconstruction from control points on base mesh (1.6 percent of coefficients, 19527 points).

We have also developed an algorithm for the automatic generation of base meshes with subdivision hierarchy for isosurfaces, see Bertram

et al. (2000b). The algorithm starts with a fine triangulation that is simplified to a coarse mesh by collapsing edges. The base mesh is a coarse, simplified mesh with some triangles merged to polygons. We recursively subdivide the base mesh, project its control points onto the original high-resolution isosurface, and relax the mesh after every subdivision step using Laplacian smoothing. We have applied this algorithm to an isosurface extracted from a high-resolution turbulent hydrodynamics simulation (Richtmeyer-Meshkov instability), courtesy of Lawrence Livermore National Laboratory. We have applied our generalized bicubic wavelet transform to the sampled isosurface (consisting of 1187277 samples at the third subdivision level) and reconstructed the surface from smaller sets of coefficients selected by thresholding, see Figure 8.

4. ACKNOWLEDGEMENTS

This work was performed under the auspices of the U.S. Department of Energy by University of California Lawrence Livermore National Laboratory under contract No. W-7405-Eng-48. In addition, this work was supported by the National Science Foundation under contracts NSF-MRI9977218, NSF-ACR-9978099, ACI 9624034 (CAREER Award), through the Large Scientific and Software Data Set Visualization (LSSDSV) program under contract ACI 9982251, and through the National Partnership for Advanced Computational Infrastructure (NPACI); the Office of Naval Research under contract N00014-97-1-0222; the Army Research Office under contract ARO 36598-MA-RIP; the NASA Ames Research Center through an NRA award under contract NAG2-1216; the Lawrence Livermore National Laboratory under ASCI ASAP Level-2 Memorandum Agreement B347878 and under Memorandum Agreement B503159; the Lawrence Berkeley National Laboratory; the Los Alamos National Laboratory; and the North Atlantic Treaty Organization (NATO) under contract CRG.971628. We also acknowledge the support of ALSTOM Schilling Robotics and Silicon Graphics, Inc. We thank the members of the Visualization Group at the Center for Image Processing and Integrated Computing (CIPIC) at the University of California, Davis.

References

- M. Bertram (2000), *Multiresolution Modeling for Scientific Visualization*, Ph.D. Thesis, University of California at Davis, July 2000.
<http://daddi.informatik.uni-kl.de/~bertram>
- M. Bertram, M.A. Duchaineau, B. Hamann, and K.I. Joy (2000a), *Wavelets on planar tessellations*, Proceedings of the 2000 International

- Conference on Imaging Science, Systems, and Technology, Las Vegas, USA, CSREA Press, 2000, pp. 619–625.
- M. Bertram, M.A. Duchaineau, B. Hamann, and K.I. Joy (2000b), *Bicubic subdivision-surface wavelets for large-scale isosurface representation and visualization*, Proceedings of IEEE Visualization '00, IEEE, 2000, pp. 389–396 & 579..
- H. Biermann, A. Levin, and D. Zorin (2000), *Piecewise smooth subdivision surfaces with normal control*, Computer Graphics, Proceedings of Siggraph 2000, ACM, to appear, 2000.
- E. Catmull and J. Clark (1978), *Recursively generated B-spline surfaces on arbitrary topological meshes*, Computer-Aided Design, Vol. 10, No. 6, Nov. 1978, pp. 350–355.
- D. Doo and M. Sabin (1978), *Behaviour of recursive division surfaces near extraordinary points*, Computer-Aided Design, Vol. 10, No. 6, Nov. 1978, pp. 356–360.
- M.A. Duchaineau (1996), *Dyadic splines*, Ph.D. thesis, Department of Computer Science, University of California, Davis, 1996.
<http://graphics.cs.ucdavis.edu/~duchaine/dyadic.html>
- M. Duchaineau, M. Wolinsky, D.E. Sigeti, M.C. Miller, C. Aldrich, and M.B. Mineev-Weinstein (1997), *ROAMing terrain: real-time optimally adapting meshes*, Proceedings of Visualization '97, IEEE, 1997, pp. 81–88 & 585.
- M. Lounsbery, T.D. DeRose, and J. Warren (1997), *Multiresolution analysis for surfaces of arbitrary topological type*, ACM Transactions on Graphics, Vol. 16, No. 1, ACM, Jan. 1997, pp. 34–73.
- J. Peters, U. Reif (1998), *Analysis of algorithms generalizing B-spline subdivision*, SIAM Journal on Numerical Analysis, Vol. 13, No. 2, SIAM, April 1998, pp. 728–748.
- P. Schröder and W. Sweldens (1995), *Spherical wavelets: efficiently representing functions on the sphere*, Computer Graphics (Proceedings of SIGGRAPH '95 Proc), Association for Computing Machinery (ACM), 1995, pp. 161–172.
- J. Stam (1998), *Exact evaluation of Catmull-Clark subdivision surfaces at arbitrary parameter values*, Computer Graphics (Proceedings of SIGGRAPH '98 Proc), Association for Computing Machinery (ACM), 1998, pp. 395–404.
- E.J. Stollnitz, T.D. DeRose, and D.H. Salesin (1996), *Wavelets for Computer Graphics—Theory and Applications*, Morgan Kaufmann Publishers, Inc., San Francisco, California, 1996.

W. Sweldens, *The lifting scheme: a custom-design construction of biorthogonal wavelets*, Applied and Computational Harmonic Analysis, Vol. 3, No. 2, pp. 186–200, 1996.

Appendix

We briefly summarize the one-dimensional construction for linear and cubic B-spline wavelets with two vanishing moments, shown in Figure 9. The corresponding scaling functions are B-splines.

Starting with a control polygon at resolution $j + 1$, defined by points c_k^{j+1} (scaling function coefficients), the fitting operator \mathbf{F} transforms every second control point into a point of c_i^j defining a control polygon for the next-coarser approximation at resolution j . The remaining points in c_k^{j+1} are transformed by the compaction-of-difference operator \mathbf{C} into wavelet coefficients d_i^j . This process is called *decomposition* or *analysis*, defined as

$$c_i^j = \sum_{k \in \mathbb{Z}} l_{k-2i} c_k^{j+1}, \tag{1.1}$$

$$d_i^j = \sum_{k \in \mathbb{Z}} h_{k-2i} c_k^{j+1}, \tag{1.2}$$

where l and h are finite discrete filters. The inverse process, called *reconstruction* or *synthesis*, is defined as

$$c_k^{j+1} = \sum_{i \in \mathbb{Z}} (\tilde{l}_{k-2i} c_i^j + \tilde{h}_{k-2i} d_i^j), \tag{1.3}$$

where the filters \tilde{l} and \tilde{h} are used to compute the subdivision operator \mathbf{S} and the expansion-of-difference operator \mathbf{E} , respectively. These four filters are shown in Table 1.

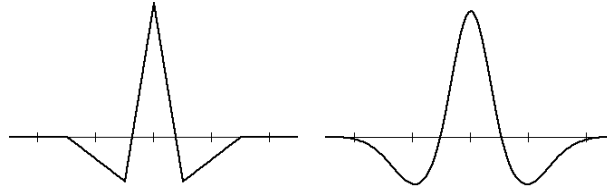


Figure 9 Linear and cubic B-spline wavelets.

degree	h_0	$h_{\pm 1}$	$h_{\pm 2}$	l_0	$l_{\pm 1}$	$l_{\pm 2}$	$l_{\pm 3}$
linear	1	$-\frac{1}{2}$		$\frac{3}{4}$	$\frac{1}{4}$	$-\frac{1}{8}$	
cubic	$\frac{3}{2}$	-1	$\frac{1}{4}$	$\frac{5}{4}$	$\frac{5}{32}$	$-\frac{3}{8}$	$\frac{3}{32}$

degree	\tilde{h}_0	$\tilde{h}_{\pm 1}$	$\tilde{h}_{\pm 2}$	$\tilde{h}_{\pm 3}$	\tilde{l}_0	$\tilde{l}_{\pm 1}$	$\tilde{l}_{\pm 2}$
linear	$\frac{3}{4}$	$-\frac{1}{4}$	$-\frac{1}{8}$		1	$\frac{1}{2}$	
cubic	$\frac{5}{8}$	$-\frac{5}{64}$	$-\frac{3}{16}$	$-\frac{3}{64}$	$\frac{3}{4}$	$\frac{1}{2}$	$\frac{1}{8}$

Table 1 Discrete decomposition and reconstruction filters for one-dimensional linear and cubic B-spline wavelets.

Instead of using formulae (1.1–1.3), we compute the wavelet transforms by small and local lifting operations. These lifting operations are more efficient to compute, and one can generalize them to arbitrary meshes in the surface case. For our linear B-spline wavelet, the one-dimensional reconstruction formula is computed by two lifting operations,

$$\begin{aligned}
 c'_i &= c_i^j - \frac{1}{4}(d_{i-1}^j + d_i^j), \\
 d'_i &= d_i^j + \frac{1}{2}(c'_i + c'_{i+1}), \quad \text{and} \\
 c_k^{j+1} &= \begin{cases} c'_{k/2} & \text{if } k \text{ is even,} \\ d'_{(k-1)/2} & \text{otherwise.} \end{cases}
 \end{aligned} \tag{1.4}$$

The one-dimensional reconstruction formula for our cubic B-spline wavelet requires three lifting operations and is defined as

$$\begin{aligned}
 c'_i &= \frac{1}{2}c_i^j - \frac{3}{16}(d_{i-1}^j + d_i^j), \\
 d'_i &= d_i^j + (c'_i + c'_{i+1}), \\
 c''_i &= c'_i + \frac{1}{4}(d'_{i-1} + d'_i), \quad \text{and} \\
 c_k^{j+1} &= \begin{cases} c''_{k/2} & \text{if } k \text{ is even,} \\ d'_{(k-1)/2} & \text{otherwise.} \end{cases}
 \end{aligned} \tag{1.5}$$

The corresponding decomposition formulae are obtained by applying the inverse of every individual lifting operation in reverse order.